Supplemental Material

Methods

Rapid Atrial Pacing Model

New Zealand White rabbits (2.5-3 kg) were anesthetized with ketamine (50 mg/kg)/xylazine (5 mg/kg) via intramuscular (i.m.) injection. After endotracheal intubation, inhalation anesthesia (1.5% isoflurane) was maintained via mechanical ventilation with a rate of ~ 30/minute. Pacemaker leads were implanted via the left and right internal jugular veins into the right atrium and left superior caval vein, respectively. After a recovery period (1 week) the right atrium was rapidly stimulated using an external pacemaker (Itrel Medtronic, 4x threshold) with a rate of 10 Hz for 5 days (Supplemental Figure 1). Only animals with AV-conduction in a 3:1 block pattern, resulting in a ventricular rate of ~200/min, which is normal for rabbits, were included in the study group. Atrial effective refractory period (AERP) was measured at different cycle lengths (240-160 ms) in awake animals prior to and after 5 days of rapid atrial pacing. AERP measurements were performed after steady-state had been established at each cycle length (2 minutes; 2 x threshold). Sham operated animals served as controls.

AF was not inducible in control or RAP rabbits using an S1-S2 protocol. After cessation of atrial pacing, all animals converted back to normal sinus rhythm.

Human Atrial Myocyte Isolation

Human atrial tissue was collected during open-heart surgery. All patients gave written informed consent prior to surgery. The study protocols were approved by the Institutional Review Board at the University of Maryland (for left atrial specimens) and the medical-ethical committee at Maastricht University (MEC 2010-

2004). The atrial specimens were stored in modified Tyrode's solution (in mmol/l NaCl 135, KCl 4.75, KH_2PO_4 1.19, Na_2HPO_4 16, HEPES 10, glucose 10, sucrose 70, $NaHCO_3$ 25, 2,3-butanedione monoxime (BDM) 30, pH 7.4, gassed with 5% CO_2/95% O_2). Atrial myocytes were isolated as described previously (1, 2). Myocardial specimens were cut into chunks (approximately $1mm^3$) and washed in Ca^{2+}-free Tyrode 2 x 5min. Afterwards, the tissue was incubated in 20 ml Ca^{2+} free Tyrode containing 220 U/ml protease XXIV (Sigma) and 50 U/ml collagenase V (Sigma) but no BDM, was kept at 37 °C and gassed with carbogen. This was followed by an incubation in a solution containing fresh collagenase V (100 U/ml) but no protease. The incubation was finished as soon as microscopic examination revealed a satisfactory number of intact myocytes. After centrifugation (100 g for 2 minutes), cardiomyocytes were re-suspended in a solution containing (mmol/l): NaCl 120, KCl 5.4, $MgSO_4$ 5, sodium pyruvate 5, glucose 20, taurine 20, HEPES 10; pH adjusted to 7.4 with NaOH. Finally, a stepwise re-exposure to Ca^{2+} was performed by increasing the $CaCl_2$ concentration every 10 minutes by 200 µmol/l to a final concentration of 1 mmol/l.

T-Tubule Staining

For cell membrane staining freshly isolated atrial myocytes (rabbit, mouse, human) were loaded with 5 µmol/l of the membrane selective fluorescent dye di-8-ANEPPS (Life Technologies) followed by a 15-minute wash-out at room temperature. Fluorescence was excited at 543 nm and the emitted signal was recorded at > 600 nm. To visualize t-tubules z-stacks of the whole cell were acquired with 0.5 µm intervals in the z dimension. Sarcolemmal surface membrane was identified in the thresholded XY images as the signal intense margin of the cell and was excluded for t-tubule signal density measurements. T-tubule signal density was then quantified as the number of signal-positive voxels within the cell margins. The middle 10 slices of the stack were used for t-tubule analysis.

Whole Cell Voltage Clamp Measurements

Only rod-shaped myocytes with clear cross-striation were used for electrophysiological measurements with the patch-clamp technique in conventional whole-cell mode using an Axopatch 200B amplifier (Molecular Devices) and a computer equipped with the Clampex and Clampfit software (Molecular Devices). For measurements of the L-type Ca^{2+} current ($I_{Ca,L}$) the bath solution contained (in mmol/l): tetraethylammonium chloride (TEA-Cl) 136, $CaCl_2$ 1.8, $MgCl_2$ 1.8, HEPES 10; pH adjusted to 7.4 with TEA-OH. The pipette solution contained: CsCl 140, $MgCl_2$ 1.7, Mg-ATP 0.3, EGTA 10, HEPES 10; pH adjusted to 7.2 with CsOH. Experiments were performed at room temperature (21-23°C). After establishing the whole-cell configuration with access resistances < 10 MΩ, cells were allowed to equilibrate until all fast inward currents and all outward currents had disappeared and $I_{Ca,L}$ currents had reached a stable plateau, as assessed by voltage ramps from -90 to +60 mV over 200 ms every 45 s. Voltage-dependent inward currents were elicited by stepwise increase in depolarizing pulses from a holding potential of -60 mV for 200 ms.

For action potential recordings, SR Ca^{2+} load and Na^+/Ca^{2+} exchanger measurements micropipettes were filled with solution containing (in mmol/l): K-glutamate 120, KCl 30, $MgCl_2$ 5, NaCl 2.8, K_2-ATP 5, Na_2-phosphocreatine 3.6, cAMP 0.05, HEPES 10 (pH 7.2, adjusted with KOH). Cells were superfused with an external solution containing (in mmol/l): NaCl 135, KCl 5.4, $CaCl_2$ 2, $MgCl_2$ 1, glucose 10, HEPES 5 (pH 7.4, adjusted with NaOH). Action potentials were initiated by depolarizing current pulses (1 ms duration, 1.5 x threshold) at a rate of 2 Hz under whole cell current clamp conditions. Glass Pipettes had resistances of 1.5-2.5 MΩ.

Quantitative Assessment of Sarcoplasmic Reticulum Ca^{2+} load

Quantitative measurements of SR Ca^{2+} load were carried out by simultaneous recordings of $[Ca^{2+}]_i$ with Fluo-3 using whole cell epifluorescence and membrane current in single cells under voltage clamp control as shown in Figure 4. Cells were loaded with Fluo-3-AM (10 μmol/l) for 20 minutes at room temperature followed by 20 minutes of de-esterification. To prevent Fluo-3 leakage during whole cell voltage-clamp experiments pipettes contained 100 μmol/l Fluo-3 free acid. Prolonged application of caffeine (10 mmol/l) activates the release of all of the Ca^{2+} in the SR, which is pumped out of the cell largely by the electrogenic sarcolemmal Na^+/Ca^{2+} exchanger (NCX). The NCX thus produces a current (I_{NCX}) which provides a quantitative measurement of NCX pumping. The integral of the resulting I_{NCX} is a quantitative measure of the amount of Ca^{2+} in the SR (3) that was extruded by NCX as shown in Figure 4. Importantly, the $[Ca^{2+}]_i$ dependence of I_{NCX} reflects the abundance of NCX function.

Non-NCX, non-Serca mediated Ca^{2+} or slow Ca^{2+} removal pathways were evaluated by inhibiting NCX with Ni^{2+} (10 mmol/l) before inducing SR Ca^{2+} depletion by caffeine (10 mmol/l). During this experiment NCX-dependent Ca^{2+} extrusion is blocked and the rate of Ca^{2+} extrusion is determined by the slow Ca^{2+} removal pathways (which consist mainly of plasma membrane Ca^{2+} ATPase). The rate of non-NCX mediated Ca^{2+} extrusion (k_{slow}) was unchanged between CTL and RAP cells (Supplemental Figure 7).

Determination of Fast intracellular Ca^{2+} Buffering Strength:

Fast application of caffeine (10 mmol/l) to voltage-clamped atrial myocytes resulted in a transient inward current, which is carried by the NCX (I_{NCX}) and driven by the transient increase of the free intracellular Ca^{2+} (4). The change of total Ca^{2+} in the cell during the slow I_{NCX} decay was obtained by the change in the reverse time integral of I_{NCX} (total $[Ca^{2+}]_i$), which was plotted against the simultaneously measured change in

free $[Ca^{2+}]_i$ (Whole cell epifluorescence, fluo-3, see above) to obtain the fast intracellular Ca^{2+} buffering strength of the cell. If diastolic $[Ca^{2+}]_i$ is unchanged (as measured independently in our study) F/F_0 can be used as a measure for free Ca^{2+} without calibration for $[Ca^{2+}]$. If F/F_0 is used, the relation between total and free Ca^{2+} during the buffering measurements is expected to remain linear. Thus, a steeper slope of the F/F_0 - total Ca^{2+} relation shows an increased Ca^{2+} buffering 'strength'.

EMD experiments:

Experiments were performed at 0.5 Hz due to the strong motion artifacts in EMD cells at higher stimulation rates. The generally lower CaT amplitudes are due to the low stimulation rate (see also Supplemental Figure 3B for rate dependence of CaT amplitude).

Western Blot Analysis

Left atrial homogenates of rabbit myocardium were obtained from frozen tissue and protein concentrations were determined with Amido-Black 10B. Proteins were fractionated on SDS-polyacrylamide gels and transferred to nitrocellulose membranes (BioTrace®NT, Life Sciences). Western blotting was performed with primary antibodies to GAPDH (CSQ, 1:2500; Dianova), troponin-C (monoclonal; 1:1000; Fitzgerald), sarcoplasmic reticulum (SR) Ca^{2+}-ATPase (Serca2a, 1:2000; Santa Cruz), Thr287-phosphorylated Ca^{2+}/calmodulin protein kinase II (pThr287-CaMKII, 1:5000; Promega), total, Ser16- and Thr17-phosphorylated phospholamban (PLB, all 1:5000; Badrilla), total ryanodine receptor (RyR2, 1: 5000), Ser2809-phosphorylated RyR2 (1:1000; kind gifts from Dr. Andrew Marks, Columbia University), PMCA (1:200) total Na+/K+ ATPase (NKA alpha5, DSHB, 1:500), total phospholemman (PLM, PLM FXYD1, abcam, 1:500), PLM-serine63 and PLM-serine68 (1:500, kind gift from Will Fuller) as previously described (5). For confirmation of reduction of RyR2 protein expression RyR2 primary antibody RYR MA3-925 was used (1:5000, Pierce, Thermo Scientific); similarly for confirmation of

increased RyR2 phosphorylation at Ser2808 the primary antibody RyR2 pSer2808 (1:2000; Badrilla) was used. For detection of RyR2 phosphorylation at Ser2814 the primary antibody RyR2 pSer2814 (1:1000; Badrilla) was used and for detection of RyR2 phosphorylation at Ser2030 the primary antibody RyR pSer2030 (1:500; kind gift from X. Wehrens) was used. Detection was obtained with suitable secondary antibodies and protein bands were visualized by electrochemiluminescence reagents (Pierce) and Hyperfilm-ECL (Amersham). Films were evaluated densitometrically with Phoretix 1D software (Biostep).

To analyze myofilament protein phosphorylation proteins were separated on a 1D-gradient gel and stained with ProQ-Diamond, which stains phosphorylated proteins (cMyBP-C, cardiac myosin binding protein C; TnT and TnI, cardiac troponin T and I; MLC2, myosin light chain 2). Gels were subsequently stained with SYPRO Ruby to analyze total protein expression.

$[Na^+]$ Measurements

Isolated myocytes were plated on laminin-coated glass coverslips mounted in perfusion chambers. Myocytes were loaded with 10 μmol/l SBFI-AM for 120 min, at 37° C, in the presence of the non-ionic surfactant Pluronic F-127 (0.05 % w/v). After washout of the external dye, SBFI-AM de-esterification was allowed for 20 minutes at room temperature before proceeding with $[Na^+]_i$ measurements. The perfusion chamber was mounted on an inverted microscope (Nikon TE2000-S). Fluorescence was elicited by illumination with a 75 W xenon lamp. Dual excitation measurements (at 340 and 380 nm; *F*340 and *F*380; alternating at 100 Hz) were performed using an IonOptix Hyperswitch and PMT (IonOptix).The raw 340 nm, 380 nm and 340/380 ratio signals were sampled at 1 kHz and displayed, stored and analyzed using IonWizard software (IonOptix). The emitted fluorescence was recorded at 510 ± 20 nm. The emission field was restricted to a single cell with a rectangular diaphragm. A linear regression of autofluorescence at each wavelength

versus two-dimensional projection of cell area for 10 unloaded cells of the same preparation was used to predict the cell size-dependent background, which was subtracted from the individual wavelength signals in SBFI-loaded cells. All measurements were performed at room temperature.

$[Na^+]_i$ Calibration

In vivo calibration of SBFI was accomplished as described by Despa (6). The SBFI loaded myocytes were exposed to various extracellular $[Na^+]$ ($[Na^+]_o$) in the presence of 10 μmol/l gramicidin D and 100 μmol/l strophanthidin. The solutions with various $[Na^+]_o$ were prepared by mixing, in different proportions, two solutions of equal ionic strength. One solution contained 145 mmol/lNa^+ (30 mmol/m NaCl, 115 mmol/l sodium gluconate) and no K^+, while the other one had 145 mmol/l K^+ (30 mmol/l KCl, 115 mmol/l potassium gluconate) and was Na^+ free. Both calibration buffers also contained 10 mmol/l Hepes, 10 mmol/l glucose and 2 mmol/l EGTA and the pH was adjusted to 7.2 with Tris base. A calibration was performed at the end of each experiment.

Ryanodine Receptor Immunocytochemistry

Freshly isolated atrial myocytes were seeded on poly-L-lysine coated glass coverslips and fixated with ice-cold methanol. For ryanodine receptor labeling cells were first washed twice with cold phosphate buffered saline (PBS, pH 7.4) and then permeabilized by washing 3 x 5 minutes with PBS containing 0.3% Triton X and 5% BSA. For labeling cells were incubated with the primary antibody raised against cardiac specific RyR2 (mouse monoclonal (C3-33), IgG1; 1:50; Affinity Bioreagents) for 90 minutes at 4 °C. The specificity of this antibody in cardiac atrial myocytes has been described previously (7). After incubation with the primary antibody the cells were again washed 3 x 5 minutes with PBS containing 0.3% Triton X and 5% BSA. The cells were then incubated with a fluorophore-conjugated secondary antibody (488 Alexa Fluor goat anti mouse; 1:200; Life Technologies) for 90 minutes at 4°C.

After the second incubation cells were washed 3 x 5 minutes with PBS containing 0.3% Triton X and 5% BSA. Coverslips were mounted with an anti-fade reagent (ProLong® Gold, Life Technologies).

Measurement of Transverse RyR2 Spacing

Confocal images were obtained using a Nikon C1 confocal laser scanning microscope (Nikon Instruments Europe B.V.) with a 40 x 1.3 numerical aperture objective corrected for the thickness of the glass coverslip. Measurements were performed according to Chen-Izu et al (8). Pixel dimensions were 0.2 x 0.2 μm in the focal plane. High-resolution images were obtained in the longitudinal section. RyR2 cluster separation was measured in the transverse spacing, which is most important for intracellular centripetal Ca^{2+} wave propagation. Measurements were only performed where RyR2 clusters were arrayed on a straight line. The spacing between RyR2 clusters is defined as the distance between peaks in the average fluorescence values. Between 4-10 ROIs were analyzed per cell. The limited axial resolution in the longitudinal section leads to a systemic underestimation of the transverse RyR2 cluster spacing (8). However, as the purpose of this study was a comparison between two groups this systemic underestimation will apply to both groups.

Measurement of RyR2 Cluster Intensity

Acquisition of confocal images was performed as described for transverse RyR2 spacing with the distinction that all images were acquired with the exact same acquisition parameters (laser power, digital gain, offset, pinhole, pixel-size and zoom) in order to compare fluorescence intensity of RyR2 clusters. To rule out intensity differences due to variability during immunostaining all cells were stained together in one experiment after testing had confirmed similar low non-specific background

staining for both groups. Prior to analyses, background subtraction was performed on each ROI using the 50 pixel rolling ball function in ImageJ.

Using the same acquisition parameters for each cell studied (laser intensity, gain, pixel size) a significant reduction in signal intensity per cluster was found in RAP cells compared to control cells (Supplemental Figure 10).

Estimation of intracellular BAPTA concentration

We have previously quantitated the loading of the indicator, Fluo-2MA, into cardiac myocytes by incubation with the corresponding AM ester at room temperature (9). BAPTA is structurally analogous to Fluo-2MA; therefore its loading into cells through incubation with the AM ester is expected to be comparable. We have found that incubation of the myocytes for 30 min with 2.5 μmol/l Fluo-2MA AM ester resulted in an intracellular Fluo-2MA concentration of 400 μmol/l (9). Assuming that intracellular loading is proportional to the AM ester concentration and the incubation time, we can estimate that incubation with 1 μmol/l BAPTA AM ester for 20 min would have achieved an intracellular BAPTA concentration of ~110 μmol/l.

Computational Modeling

Simulations were performed as shown previously (10). Ca^{2+} sparks were modeled using a whole-cell model for Ca^{2+}-induced Ca^{2+} release (CICR) in cardiac myocytes where RyR2 cytosolic $[Ca^{2+}]_i$ sensitivity and luminal SR [Ca] $([Ca^{2+}])_{sr}$ dependency have been constrained to reproduce recently reported single channel gating behavior. Consistent with Supplemental Figure 12 the model contains 20,000 independent Ca^{2+} release units (CRUs), each containing a cluster of stochastically gating RyR2s that are instantaneously coupled via local subspace [Ca] ([Ca]ds). These CRUs are coupled via a bulk myoplasmic $[Ca]_i$, which also includes a small fraction (5%) of diffusely distributed, non-junctional or ‘‘rogue’’ RyR2s. Serca2a

pumps Ca^{2+} from the myoplasm back into the SR. The SR itself is composed of junctional SR (JSR) and network SR (NSR) components, each with appropriate volumes and Ca^{2+} buffers. Each Ca^{2+}-activated RyR2 is represented by a two-state Markov chain containing one closed (C) and one open (O) state. Transitions from C to O are dependent on both $[Ca^{2+}]_{ds}$ and junctional SR [Ca] ($[Ca^{2+}])_{jsr}$, with k^+ as the association rate constant for [Ca]ds binding with units of $umol/l^{-1}\ s^{-1}\ \eta^{-1}$ and k^- as the corresponding dissociation rate constant - in s^{-1} and η is the cooperativity of Ca^{2+} binding. A luminal regulation function (ϕ) serves to modify the channel opening rate where $[Ca^{2+}]_{sr}$ is the luminal [Ca] associated with each RyR2 (which is $[Ca^{2+}]_{jsr}$ and $[Ca^{2+}]_{nsr}$ for junctional and non-junctional RyR2s, respectively). L-type Ca^{2+} channels (LCC) have been disabled for this simulation that focuses on diastolic Ca^{2+} signaling when LCCs are quiescent. For Ca^{2+} simulations with hyperphosphorylated RyR2, the opening rate (k^+) of RyR2s was doubled, assuming increased but not maximal phosphorylation (11). The resulting shift in RyR2 Ca^{2+} sensitivity is shown in Supplemental Figure 11A.

Results

Recovery of Centripetal Ca^{2+} Wave after Rest

The first stimulated CaT after a 20s rest period led to an increase in the cc/ss transient ratio in RAP cells comparable to values found during steady-state in control cells (Supplemental Figure 4). Cell width was larger in RAP compared to control but did not correlate with failure of wave propagation (Supplemental Figure 4C).

Table 1: Patient Characteristics

	CTL	**AF**
Patients, n	9	10
Gender, m/f	4/5	8/2
Age, y	62±4	67±3
Coronary Artery Disease (CAD)	3	4
Mitral Valve Disease (MVD) / Aortic Valve Disease (AVD)	5	5
CAD+VD	1	1
Hypertension	7	8
Diabetes	2	4
Hyperlipidemia	5	8
Left Ventricular Ejection Fraction (LVEF, %)	46.6±5.3	46.7±5.5
Nitrates, n	2	2
β-Blockers, n	**3**	**8***
Digoxin, n	**0**	**5***
Calcium antagonists, n	0	1
ACE inhibitor, n	0	1
AT1 blockers, n	1	3
Diuretics, n	4	7
Statins, n	4	5
Metformin, n	2	3
Insulin, n	1	1

*$p<0.05$

References

1. Skasa M, Jüngling E, Picht E, Schöndube F, and Lückhoff A. 2001. L-type calcium currents in atrial myocytes from patients with persistent and non-persistent atrial fibrillation. *Basic Res Cardiol.* 96:151-159.
2. Greiser M, Halaszovich CR, Frechen D, Boknik P, Ravens U, Dobrev D, Lückhoff A, and Schotten U. 2007. Pharmacological evidence for altered src kinase regulation of I (Ca,L) in patients with chronic atrial fibrillation. *Naunyn Schmiedebergs Arch Pharmacol.* 375:383-392.
3. Varro A, Negretti N, Hester SB, and Eisner DA. 1993. An estimate of the calcium content of the sarcoplasmic reticulum in rat ventricular myocytes. *Pflugers Arch.* 423:158-160.
4. Berlin JR, Cannell MB, and Lederer WJ. 1989. Cellular origins of the transient inward current in cardiac myocytes. Role of fluctuations and waves of elevated intracellular calcium. *Circ Res* 65:115-126.
5. El-Armouche A, Boknik P, Eschenhagen T, Carrier L, Knaut M, Ravens U, and Dobrev D. 2006. Molecular determinants of altered Ca2+ handling in human chronic atrial fibrillation. *Circulation* 114:670-680.
6. Despa S, Islam MA, Pogwizd SM, and DM. B. 2002. Intracellular [Na+] and Na+ pump rate in rat and rabbit ventricular myocytes. *J Physiol* 539:133-143.
7. Izu LT MS, Shadid JN, Chen-Izu Y, Balke CW. 2006. Interplay of ryanodine receptor distribution and calcium dynamics. *Biophys J* 91:95-112.
8. Chen-Izu Y MS, Ward CW, Soeller C, Allen BM, Rabang C, Cannell MB, Balke CW, Izu LT. 2006. Three-dimensional distribution of ryanodine receptor clusters in cardiac myocytes. *Biophys J* 91:1-13.
9. Hagen BM, Boyman L, Kao JP, and Lederer WJ. 2012. A comparative assessment of fluo Ca2+ indicators in rat ventricular myocytes. *Cell Calcium* 52:170-181.
10. Williams GS, Chikando AC, Tuan HT, Sobie EA, Lederer WJ, and Jafri MS. 2011. Dynamics of calcium sparks and calcium leak in the heart. *Biophys J* 101:1287-1296.
11. Carter S, Colyer J, and Sitsapesan R. 2006. Maximum phosphorylation of the cardiac ryanodine receptor at serine-2809 by protein kinase a produces unique modifications to channel gating and conductance not observed at lower levels of phosphorylation. *Circ Res* 98:1506-1513.

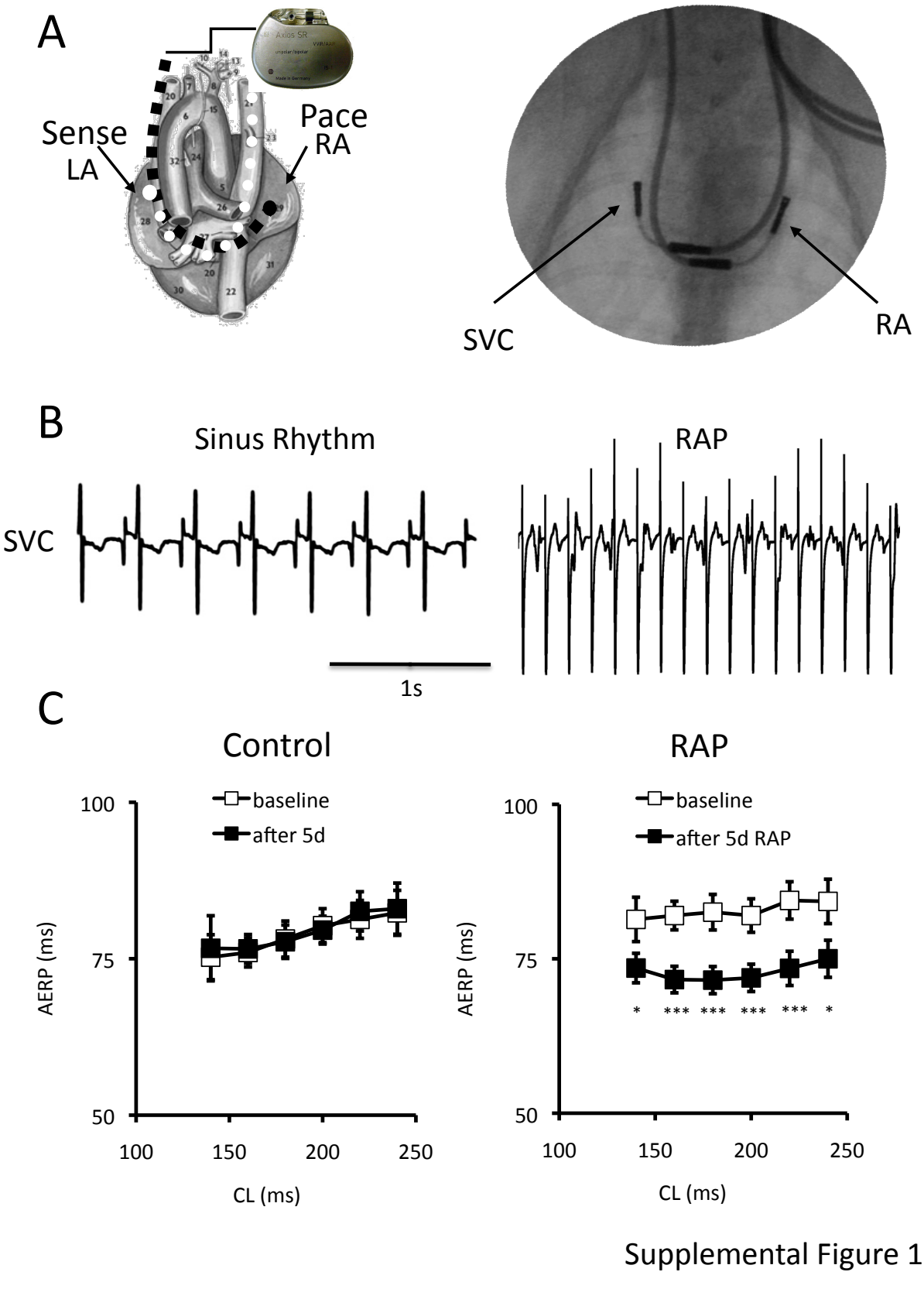

Supplemental Figure 1

Supplemental Figure 1:

RAP rabbit model and in-vivo electrophysiology. A: Schematic of pacemaker lead implantation and radiograph of pacemaker leads in the right atrium (RA) and left superior caval vein (SVC). **B:** Original left atrial (LA) electrogram recorded from the superior caval vein during sinus rhythm (left panel) and rapid atrial pacing (RAP, right panel). **C:** In-vivo recordings of atrial effective refractory period (AERP) at baseline and after 5 days (control) and at baseline and after 5 days of RAP (CTL n = 15 animals; RAP n = 17 animals).*: $p < 0.05$; ***: $p < 0.001$.

Supplemental Figure 2

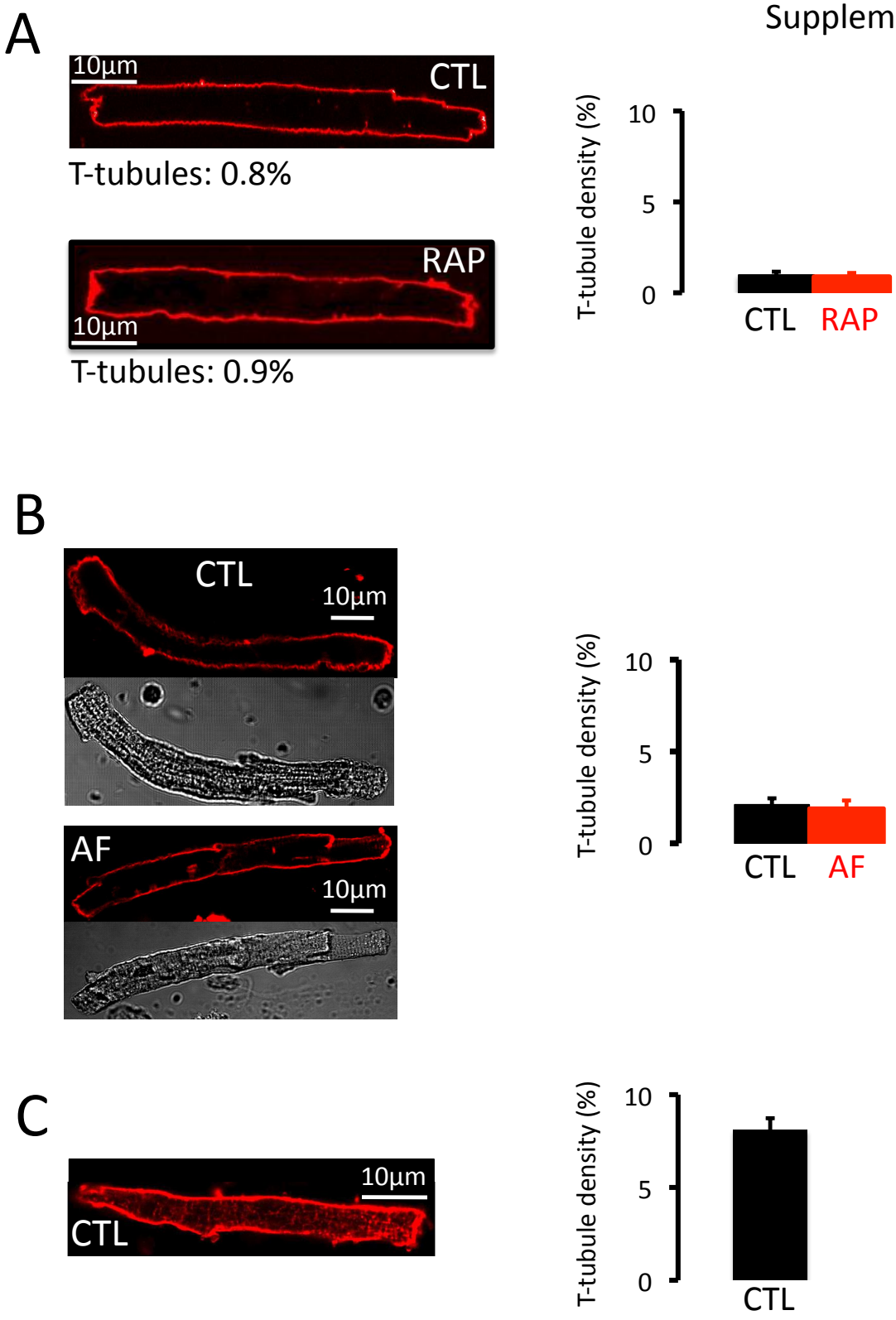

Supplemental Figure 2:
Evaluation of transverse-tubule (TT) density. A: Di-8-ANEPPS membrane staining in a rabbit left atrial control and RAP cell. There are no functionally relevant TT structures in rabbit atrial myocytes in CTL or RAP (CTL: n = 21 cells; RAP: n = 23 cells). **B:** Di-8-ANEPPS membrane staining and respective transmitted light images of human left atrial myocytes from AF patients and matched control patients in sinus rhythm (CTL: n = 21 cells, 5 patients; AF: n = 25 cells, 6 patients). Density analysis shows similar TT density in cells from patients with sinus rhythm and AF. **C:** Di-8-ANEPPS membrane staining in a mouse left atrial myocyte shows significant abundance of TTs (n = 16 cells, 3 animals).

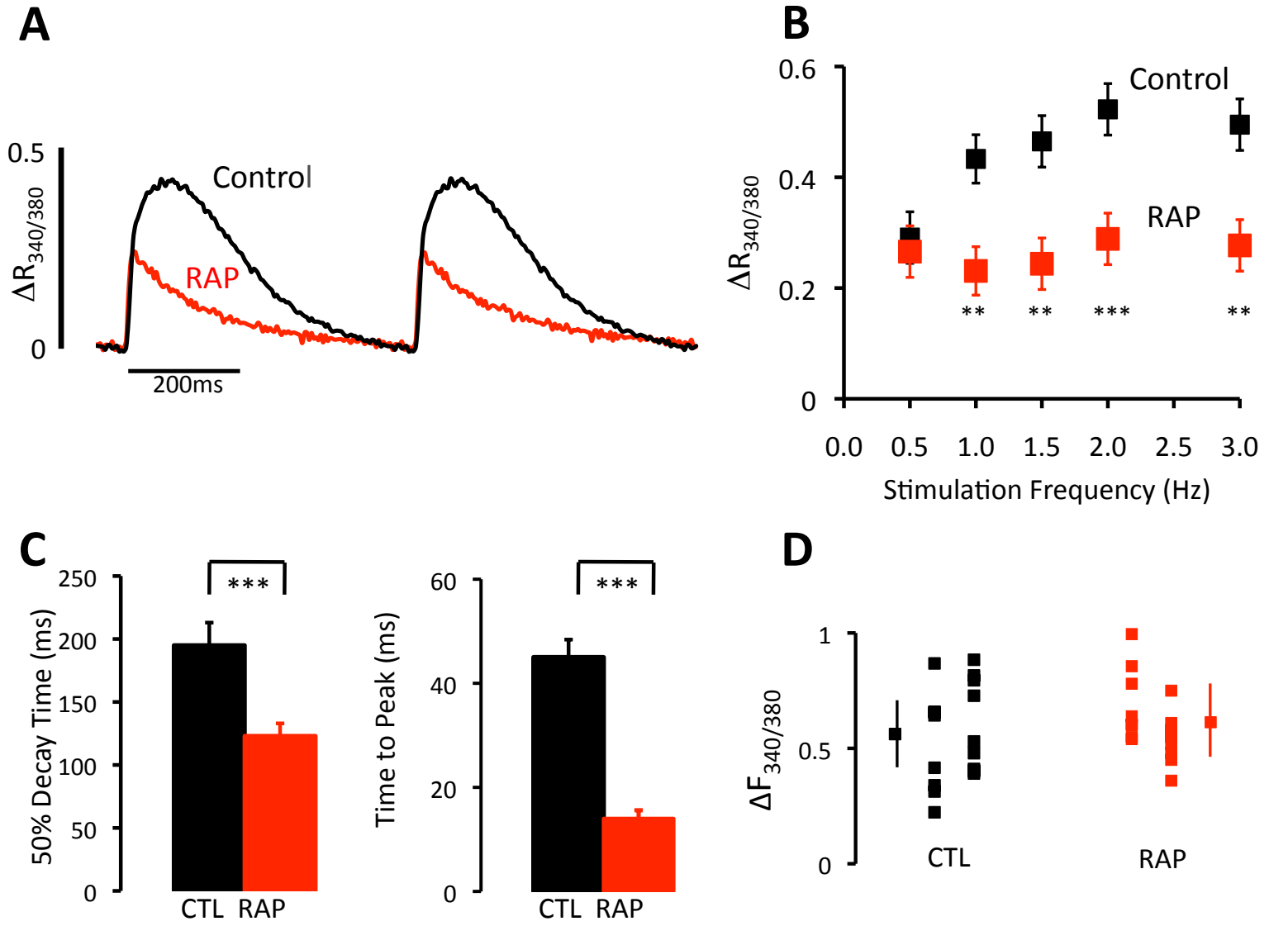

Supplemental Figure 3

Supplemental Figure 3:

Whole cell Ca^{2+} transients. A: Averaged whole cell Ca^{2+} transients from control and RAP cells (n = 10). **B:** Reduced whole cell Ca^{2+} transient amplitude and loss of frequency-dependent increase in Ca^{2+} transient increase in RAP. **C:** Altered whole cell Ca^{2+} transient kinetics in RAP. The left panel shows the shortened whole cell Ca^{2+} transient decay, the right panel shows the reduced time to peak. **D:** Diastolic cytoplasmic $[Ca^{2+}]_i$ (CTL n = 16 cells, 7 animals; RAP n = 15 cells, 6 animals) was unchanged between groups.

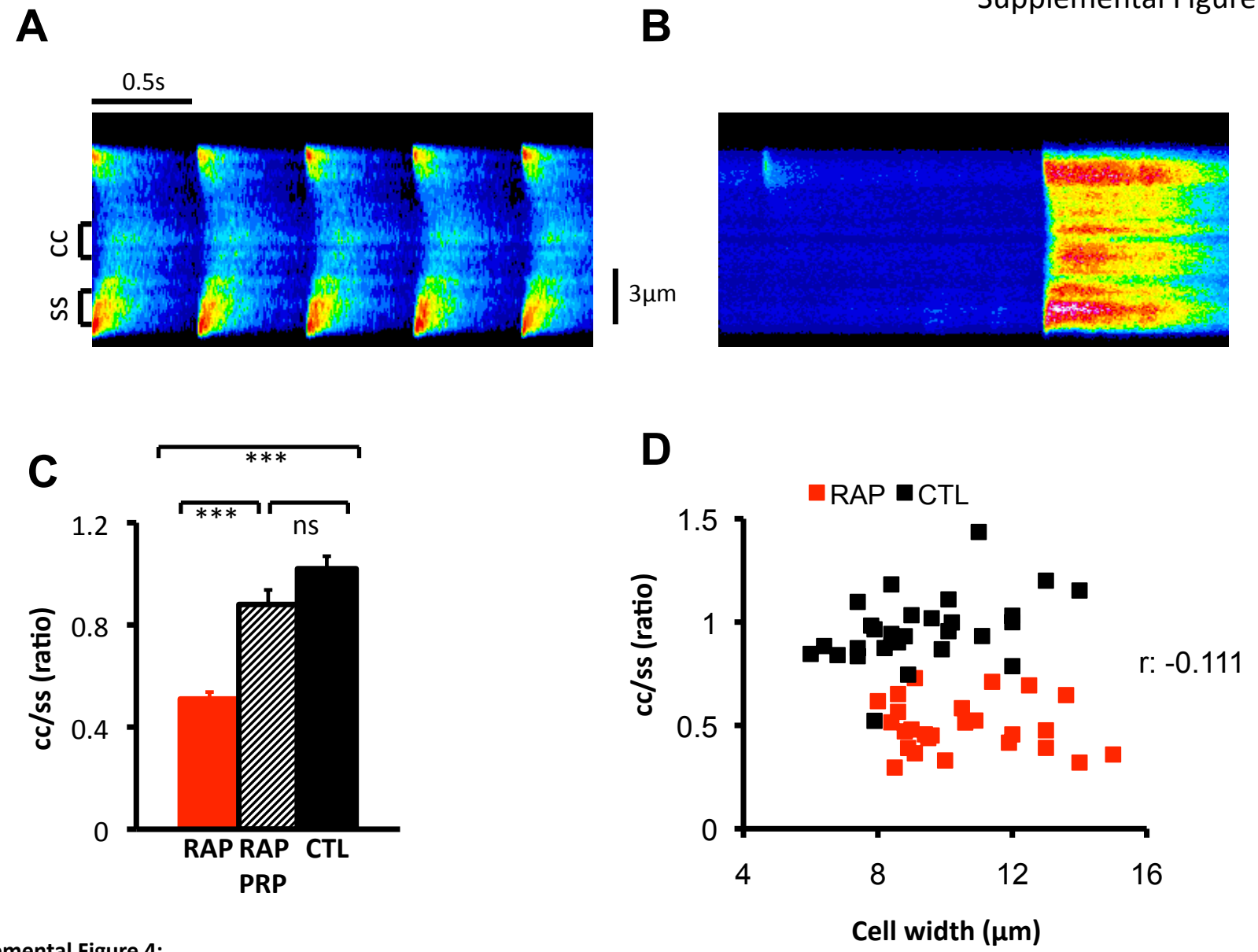

Supplemental Figure 4:

Post-rest potentiation and cell width: A: Confocal line scan recorded from an RAP cell during steady-state field stimulation (2 Hz). **B:** The line scan image shows the first stimulated beat after a 20 s stimulation pause recorded from the same cell shown in A. **C:** The central-cellular/subsarcolemmal Ca^{2+} transient ratio after a 20 s stimulation pause in RAP cells reaches similar values as steady-state Ca^{2+} transients in CTL cells (CTL: n = 28 cells, 6 animals; RAP: n = 14 cells, 5 animals). **D:** No correlation between increased cell width in RAP (CTL: 9.3 ± 0.4 µm, n = 28; RAP: 10.5 ± 0.4 µm, n = 26, $p < 0.05$) and failure of intracellular centripetal Ca^{2+} wave propagation (i.e. reduced cc/ss Ca^{2+} transient ratio). PRP: Post-rest potentiation; cc: central-cellular; ss: subsarcolemmal. ***: $p < 0.001$, ns: non-significant

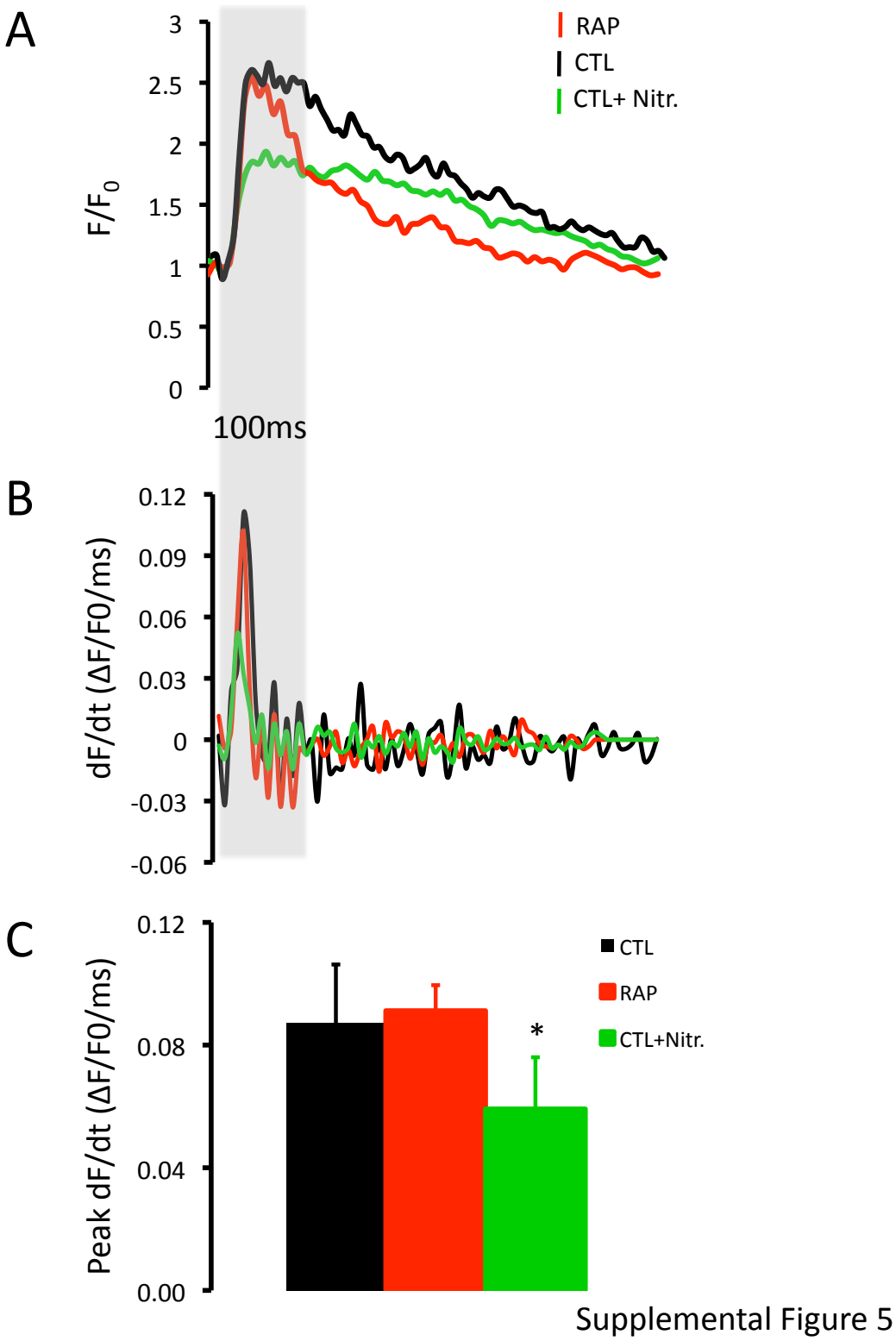

Supplemental Figure 5

Subsarcolemmal Ca^{2+} transients and SR Ca^{2+} release fluxes. A: Subsarcolemmal Ca^{2+} transients derived from confocal linescan images from CTL and RAP cells and CTL cells in the presence of nitrendipine (CTL+nitr.; 0.3 μmol/l). **B:** First derivatives of Ca^{2+} transients depicted in A showing subsarcolemmal SR Ca^{2+} release fluxes. **C:** Subsarcolemmal SR Ca^{2+} release fluxes were similar in CTL and RAP cells but significantly decreased in CTL cells in the presence of nitrendipine (CTL: n = 13 cells; CTL+nitr.: n = 13 cells; RAP: n = 14 cells). * $p < 0.05$.

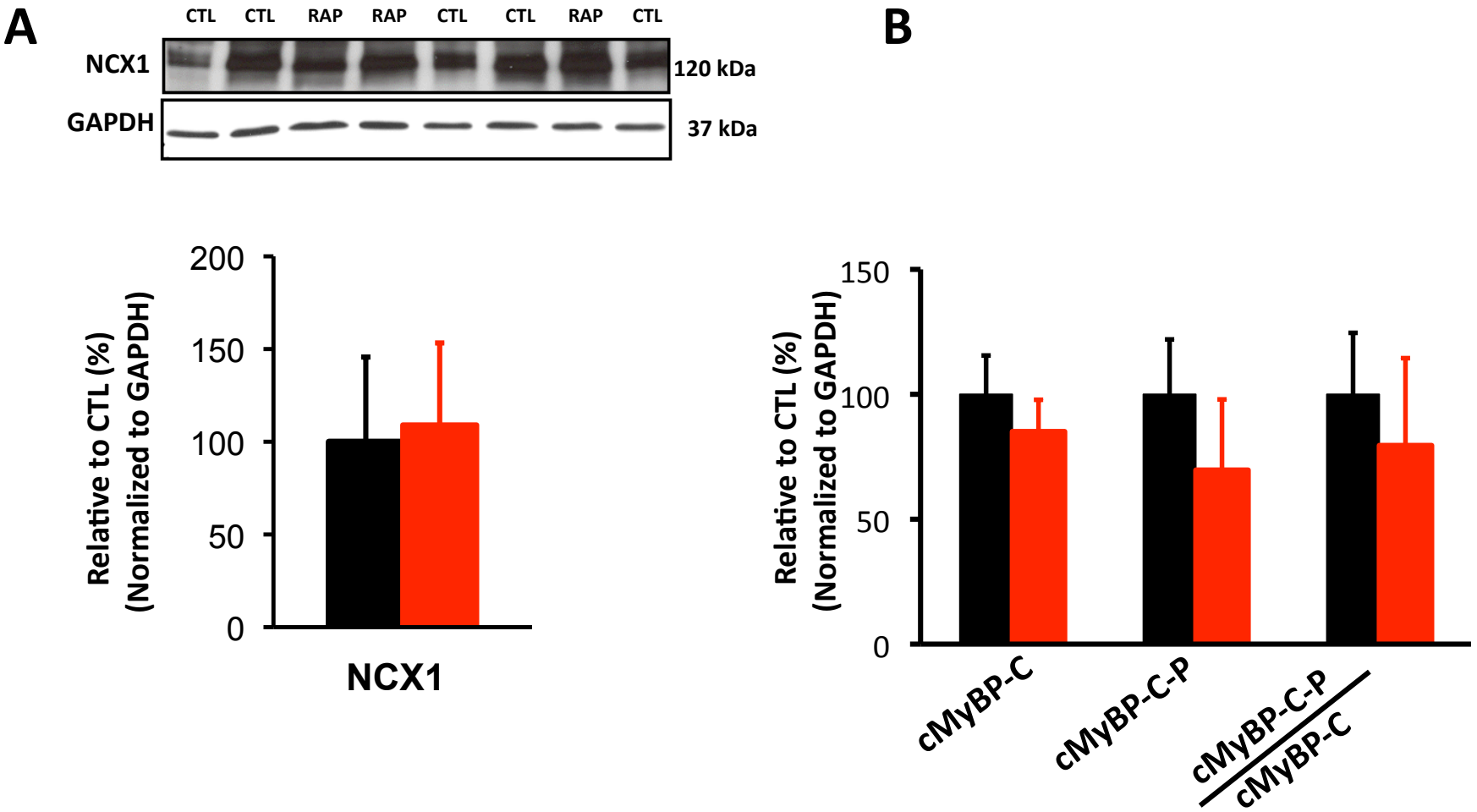

Supplemental Figure 6

Supplemental Figure 6:
Expression levels of key Ca^{2+} handling proteins: A: Protein expression levels of NCX1 were unchanged between RAP and control (relative to control and normalized to GADPH; CTL: N = 9; RAP: N = 7). N = number of animals. **B:** Protein expression and phosphorylation levels of myosin binding protein C (MyBC and MyBC-P, respectively) were unchanged in RAP (relative to control and normalized to GADPH; CTL: N = 9; RAP: N = 7).

Supplemental Figure 7

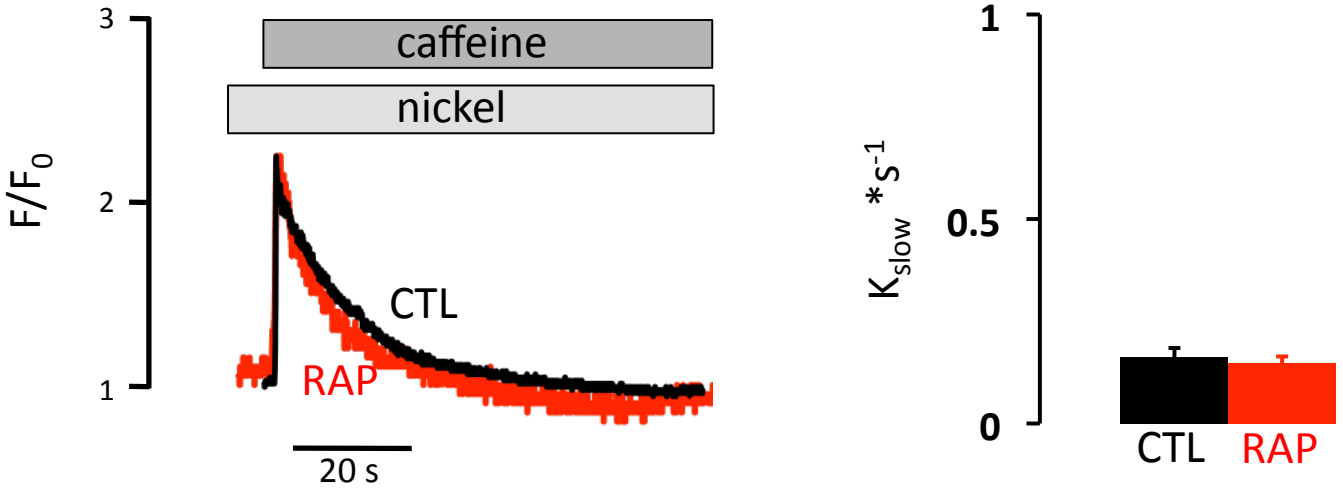

Supplemental Figure 7:
Evaluation of slow Ca^{2+} extrusion mechanisms. Experimental time course to determine the contributions made to Ca^{2+} removal by 'slow' Ca^{2+} extrusion mechanisms (PMCA). Caffeine (10 mmol/l) and nickel (10 mmol/l) applied as indicated by the horizontal bars. The right panel shows the mean data of rate decay during caffeine and nickel application (CTL: n = 12 cells, 3 animals; RAP: n = 8 cells; 3 animals).

Supplemental Figure 8

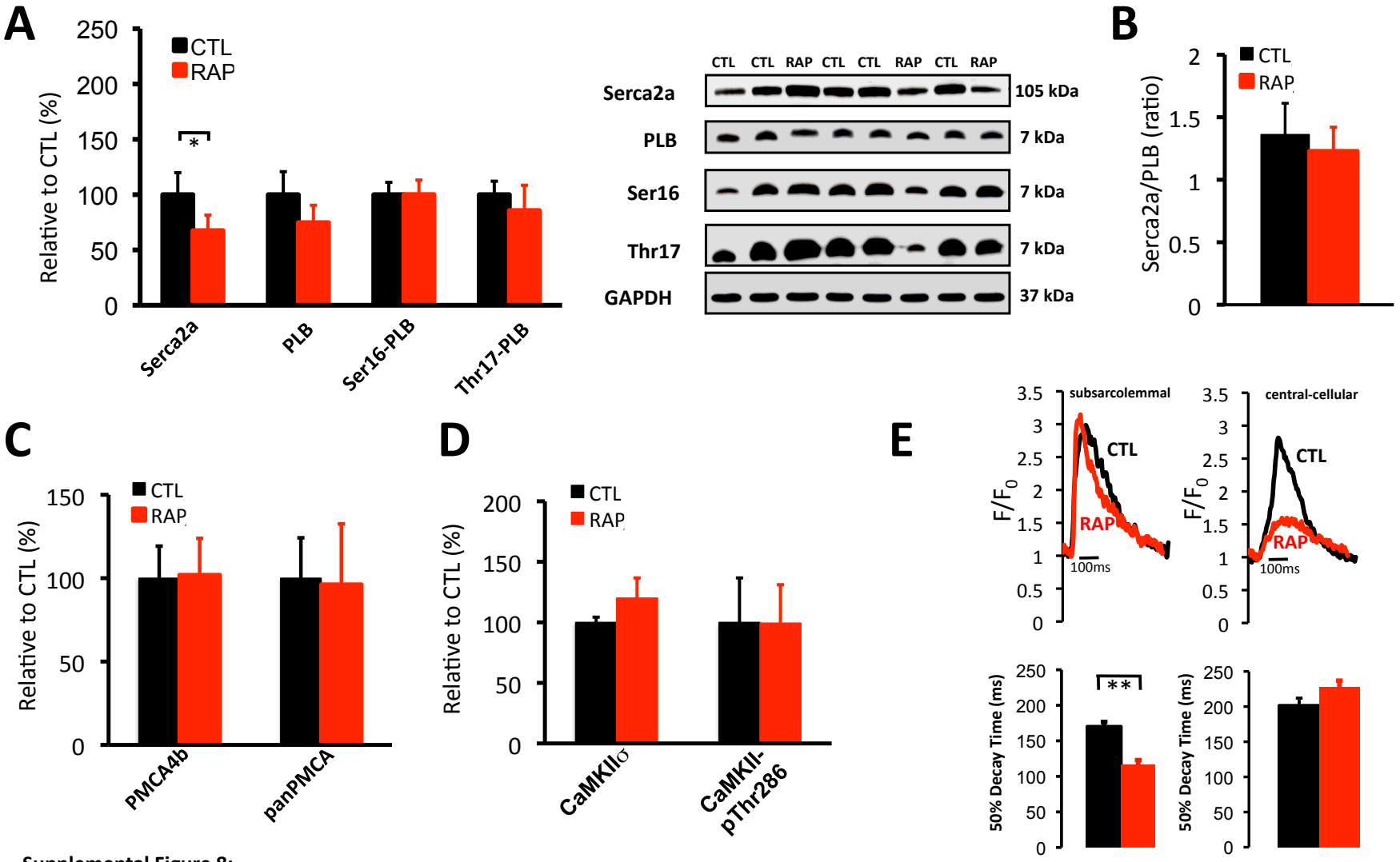

Supplemental Figure 8:
Expression levels of key Ca^{2+} handling proteins and compartmental Ca^{2+} transients: A: Protein expression levels of Serca2a, phospholamban (PLB), PKA mediated PLB phosphorylation (Ser16) and CaMKII mediated PLB phosphorylation (Thr17). Serca2a was reduced by 30% in RAP (relative to control and normalized to GADPH; CTL: N = 9; RAP: N = 7). **B:** The Serca2a/PLB ratio was unchanged in RAP. Ratios were calculated from absolute values of Serca2a and PLB (CTL: N = 9; RAP: N = 7). **C:** Protein expression levels of the plasmalemmal Ca^{2+} ATPase (PMCA) isoform 4a and panPMCA expression levels (CTL: N = 10; RAP: N = 8). **D:** Protein expression levels of CaMKIIδ and auto-phosphorylated CaMKII (Thr286) were unchanged between control and RAP (CTL: N = 9, RAP: N = 7). *:$p < 0.05$. **E:** Upper left panel: Subsarcolemmal (ss) CaTs derived from confocal linescan images from an RAP and a control cell. Upper right panel: Central-cellular (cc) CaTs derived from confocal linescan images from an RAP and a control cell. Lower panels: RAP CaT decay is faster in RAP only in the ss but not in the cc domain (CTL: n = 20 cells, N = 6; RAP: n = 18 cells, N = 5). *: $p < 0.05$; **: $p < 0.01$. N = number of animals.

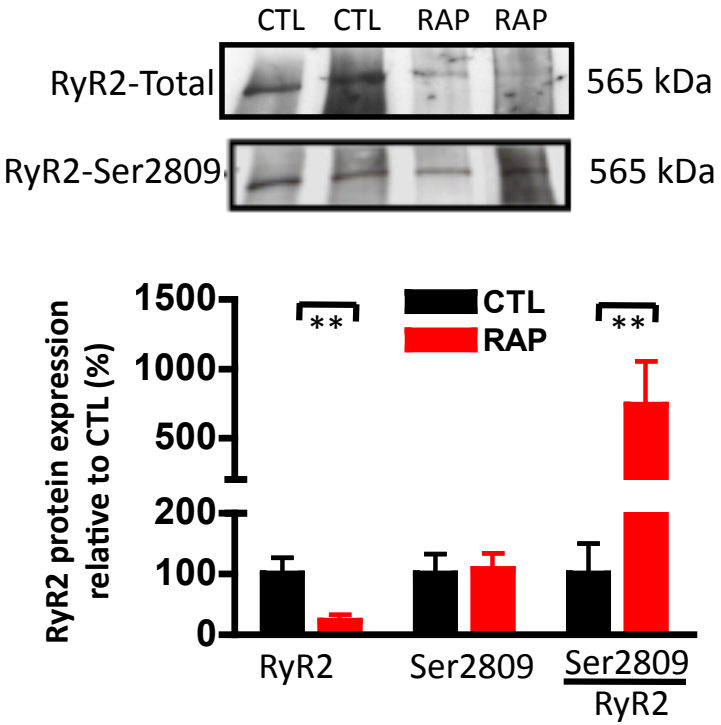

Supplemental Figure 9

RyR2 protein expression and phosphorylation: Western Blot analyses were performed with different antibodies (to RyR2 and RyR2 Ser2809) to confirm reduction of total RyR2 protein expression levels and increased phosphorylation of RyR2 at Ser2809 (as shown in Figure 8; relative to control and normalized to GAPDH; CTL: N = 8; RAP: N = 7). **:$p < 0.01$. N = number of animals.

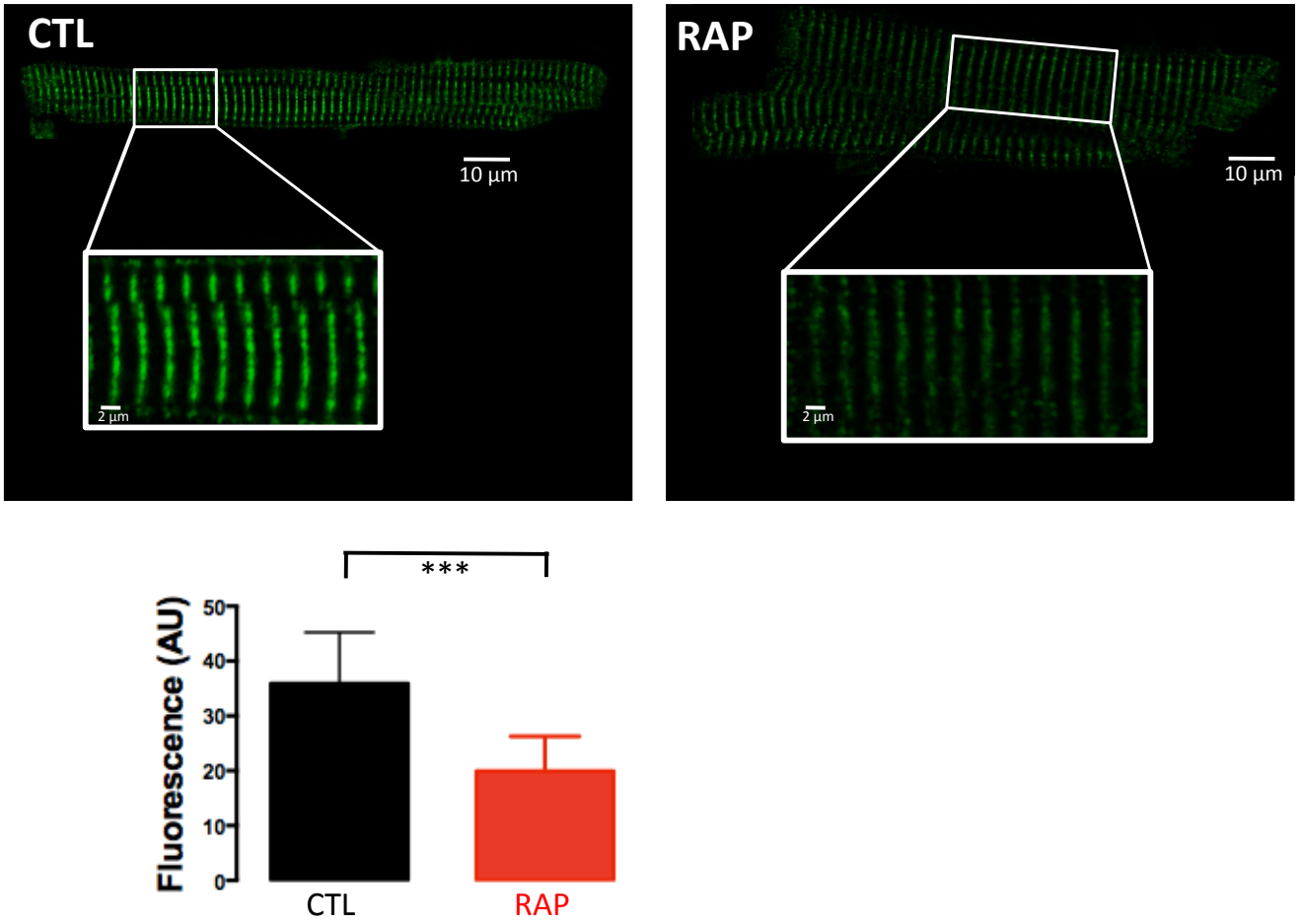

Supplemental Figure 10:
Reduced RyR2 cluster intensity in RAP. Representative confocal immunofluorescence image of a CTL cell (Upper left panel) and RAP cell (Upper right panel). Single RyR2 cluster intensity was analyzed. Mean single cluster intensity was reduced in RAP cells compared to control cells (CTL: 424 RyR2 clusters analyzed from 31 ROIs, n = 12 cells, N = 5 animals; RAP: 450 clusters were analyzed from 30 ROIs, n = 12 cells, N = 5 animals). Data are presented as means ± SD. ***: $p < 0.001$.

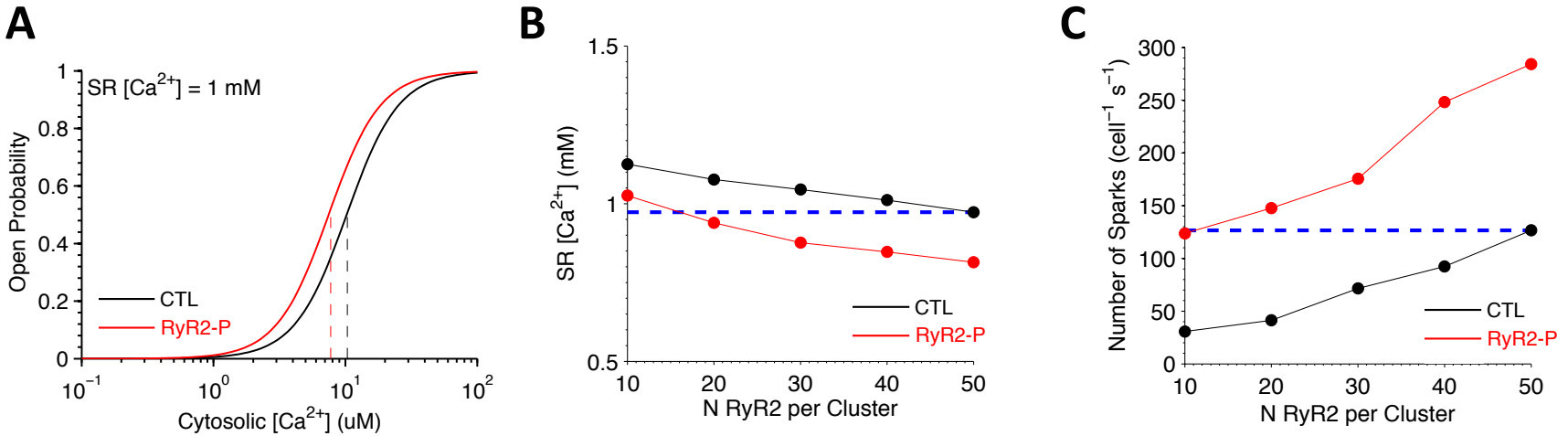

Supplemental Figure 11:
Estimating changes in Ca^{2+} spark frequency due to RyR2 remodeling using a computational model. A: Changes in RyR2 P_O used to simulate phosphorylation of RyR2 (RyR2-P, red line) along with control conditions (CTL, black line). Note, dotted lines denote EC_{50} values. **B:** Model predicted SR Ca^{2+} content for CTL (black line and circles and RyR2-P (red line and circles) as a function of CRU RyR2 density (N RyR2) where **C:** Model prediction of whole-cell Ca^{2+} spark rate as a function of CRU RyR2 density (N RyR2) for RyR2-P (red line and circles) and CTL (black line and circles) conditions. Dotted blue lines in **(B)** and **(C)** denote similar SR Ca^{2+} load and Ca^{2+} spark frequency for CTL with normal RyR2 cluster size and RyR2-P with reduced RyR2 cluster size (as in RAP).

Supplemental Figure 12

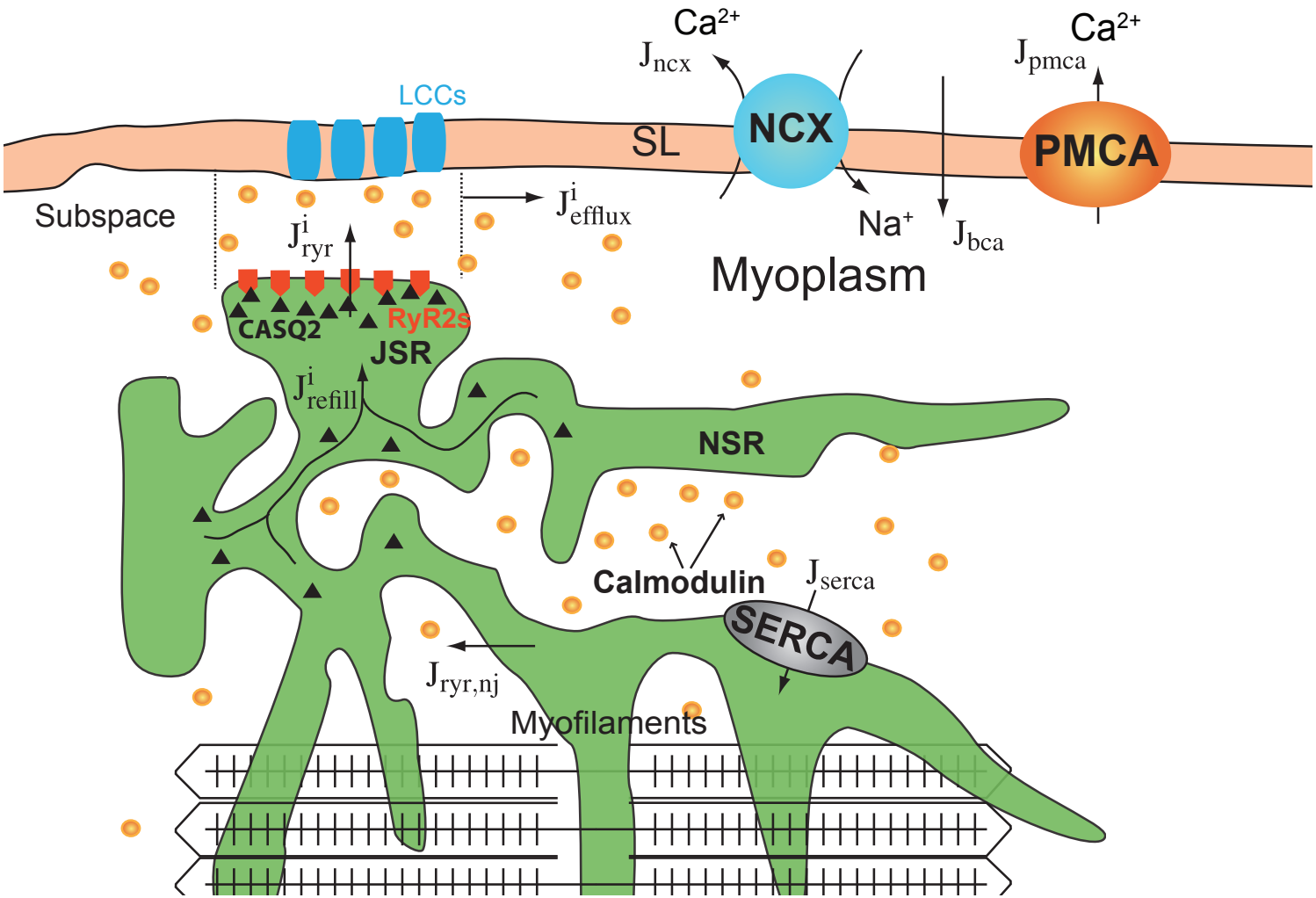

Supplemental Figure 12

Diagram of SR Ca^{2+} leak model and release site schematic. Model compartments and Ca^{2+} fluxes (solid arrows). SL: Sarcolemma; LCC: L-type Ca^{2+} channel; CASQ2: calsequestrin; JSR: junctional sarcoplasmic reticulum; NSR: non-junctional sarcoplasmic reticulum; RyR2: ryanodine receptor type 2; SERCA: sarcoplasmic reticulum Ca^{2+} ATPase; NCX: Na^{+}/Ca^{2+} exchanger; PMCA: plasma membrane Ca^{2+} ATPase.